

Spatially resolved optical emission of cubic GaN/AlN multi-quantum well structures

D.J. As¹, R. Kemper¹, C. Mietze¹, T. Wecker¹, J.K.N. Lindner¹, P. Veit², A. Dempewolf²,
F. Bertram², J. Christen²

¹Department Physik, Universität Paderborn, Warburger Strasse 100, 33095 Paderborn, Germany

²Institut für Experimentelle Physik, Universität Magdeburg, P.O. Box 4120, D-39016
Magdeburg, Germany

ABSTRACT

In this contribution we report on the optical properties of cubic AlN/GaN asymmetric multi quantum wells (MQW) structures on 3C-SiC/Si (001) substrates grown by radio-frequency plasma-assisted molecular beam epitaxy (MBE). Scanning transmission electron microscopy (STEM) and spatially resolved cathodoluminescence (CL) at room temperature and at low temperature are used to characterize the optical properties of the cubic AlN/GaN MQW structures. An increasing CL emission intensity with increasing film thickness due to the improved crystal quality was observed. This correlation can be directly connected to the reduction of the linewidth of x-ray rocking curves with increasing film thickness of the c-GaN films. Defects like stacking faults (SFs) on the {111} planes, which also can be considered as hexagonal inclusions in the cubic crystal matrix, lead to a decrease of the CL emission intensity. With low temperature CL line scans also monolayer fluctuations of the QWs have been detected and the observed transition energies agree well with solutions calculated using a one-dimensional (1D) Schrödinger-Poisson simulator.

INTRODUCTION

For advanced optoelectronic and electronic devices, like light emitting diodes (LEDs), or laser diodes (LDs) Al containing cladding layers or barriers are necessary. The commonly used hexagonal Al_yGa_{1-y}N/GaN heterostructures show an inherently strong spontaneous polarization oriented along the hexagonal c-axis as well as strain induced piezoelectric polarization. Such polarization induced electric fields in strained quantum wells can cause the spatial separation of electrons and holes resulting in a severe reduction of optical recombination efficiency [1]. Using the metastable cubic modifications of AlN and GaN such piezoelectric effects can be avoided if the samples are grown in (001) direction [2].

In general, one key issue in device fabrication is the improvement of the structural quality, because extended defects like dislocations reduce the device performance. Due to a lack of cubic GaN bulk substrates [3] 3C-SiC (001) with a mismatch of -3.5% between cubic GaN (c-GaN) and 3C-SiC is the substrate of choice. Transmission electron microscopy (TEM) measurements provide the evidence that stacking faults (SFs) on the {111} planes are the predominant crystallographic defects in c-GaN films [4,5]. These SFs are local deviations from the cubic (111) stacking sequence to the (0001) stacking sequence in the wurtzite (WZ) phase. Therefore, SFs can lead to hexagonal inclusions [6]. In the opposite case, basal-plane SFs in a WZ crystal also produce cubic inclusions in the hexagonal crystal structure. Detailed information about the

emission lines from these SFs in the WZ phase can be found in [7, 8] and the role of extended defects is studied for example in Ref. [9].

Until now the direct influence of planar defects on the CL emission characteristics of cubic GaN/AlN multi-quantum wells (c-GaN/AlN MQWs) are only scarcely reported. Therefore, we investigate the correlation between $\{111\}$ SFs and the emission intensity of c-MQW films by simultaneously measuring scanning TEM (STEM) images and CL signals at room temperature and at low temperatures [10].

EXPERIMENT

The cubic III-nitrides multi quantum well structures were grown by means of plasma-assisted molecular beam epitaxy (MBE). The used substrates consist of $12\ \mu\text{m}$ thick 3C-SiC (001) layers which were deposited by low-pressure chemical vapor deposition on a $500\ \mu\text{m}$ Si (001) substrate [11]. The growth of c-GaN was realized under one monolayer Ga on the surface and the c-AlN was grown under one monolayer Al on the surface. The absorption and desorption of the Ga and the Al layers were monitored by *in-situ* reflection high-energy electron diffraction (RHEED). Detailed information about the optimized growth conditions are given in Ref. [12, 13]. The samples were fabricated with a structure as displayed in Fig. 1. The growth direction is the [001] direction. The samples are built up of a $50\ \text{nm}$ c-GaN buffer layer on the 3C-SiC/Si (001) substrate followed by 40 periods of asymmetric QWs. The active regions are embedded in $3\ \text{nm}$ c-AlN barriers and formed by a $2.1\ \text{nm}$ c-GaN QW coupled by a $0.9\ \text{nm}$ c-AlN barrier with a $1.6\ \text{nm}$ c-GaN QW. Altogether the c-MQW films on top of the c-GaN buffer have a total thickness of around $307\ \text{nm}$.

After growth the samples were characterized by simultaneously measuring STEM images and CL signals at room temperature and $16\ \text{K}$. To this end the samples were prepared using a conventional cross-section preparation process with different steps including mechanical grinding and polishing followed by an ion beam thinning step. Before STEM analysis the samples were cleaned in an oxygen plasma and then examined in a Tecnai F20 (S)TEM operating at $80\ \text{kV}$ with an integrated CL setup. The CL system is equipped with a Mono CL4 monochromator from Gatan. Within the STEM/CL mode the excitation resolution is about $1\ \text{nm}$ at room temperature and $< 5\ \text{nm}$ at $12\ \text{K}$. The lateral resolution of the CL signal with an estimated specimen thickness of $150\text{-}200\ \text{nm}$ of the cross-section TEM specimens is determined to about $< 20\ \text{nm}$. The effect of charge carrier diffusion should be also considered, but is not quantified here.

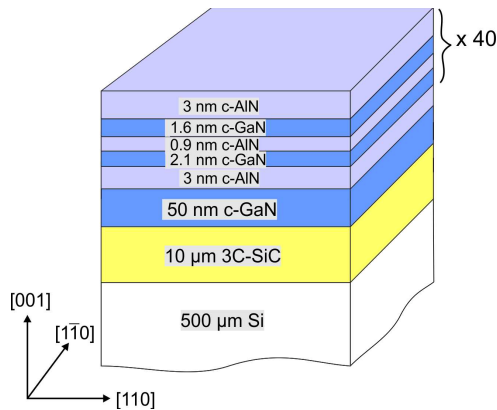


Figure 1 Structure of the cubic GaN/AlN MQW sample.

RESULTS AND DISCUSSION

Figure 2a shows a cross-sectional high-angle annular dark field (HAADF) STEM image taken along the [110] zone axis of the cubic GaN/AlN MQW sample. On top of the $50\ \text{nm}$ c-GaN buffer the MQW layer stack can be seen. In the HAADF-STEM mode the c-GaN layers can

be clearly distinguished from c-AlN by their higher intensity. The STEM image shows slight image distortions in the vertical scanning direction, visible by the rough appearance of the atomically sharp GaN/SiC interface (compare Fig. 3). For the conclusions on the optical emission properties of the sample, which will be presented in the following, these image distortions are not important. Besides the images distortions the entire MQW film exhibits undulations of the individual MQW layers. These undulations are caused by the surface shape of the c-GaN buffer and by bunches of SFs extending from the c-GaN/SiC interface up to the surface, as previous TEM studies [14] have shown. These TEM studies also revealed that SFs emerging from the substrate interface are not stopped at the c-AlN/GaN interfaces of the different layers and lead to the undulation of MQWs. In regions without any planar defects a straight sequential arrangement of c-GaN and c-AlN layers can be noticed with equal growth rate [14]. Again, a decreasing SF density with increasing film thickness due to annihilation processes can be noticed.

To analyze the influence of SFs on the luminescence output of the MQW film a panchromatic image within a wavelength range of 160-930 nm of the CL emission intensity is displayed in Fig. 2b. This image is spatially correlated to the STEM image in Fig. 2a and both images were collected simultaneously at room temperature.

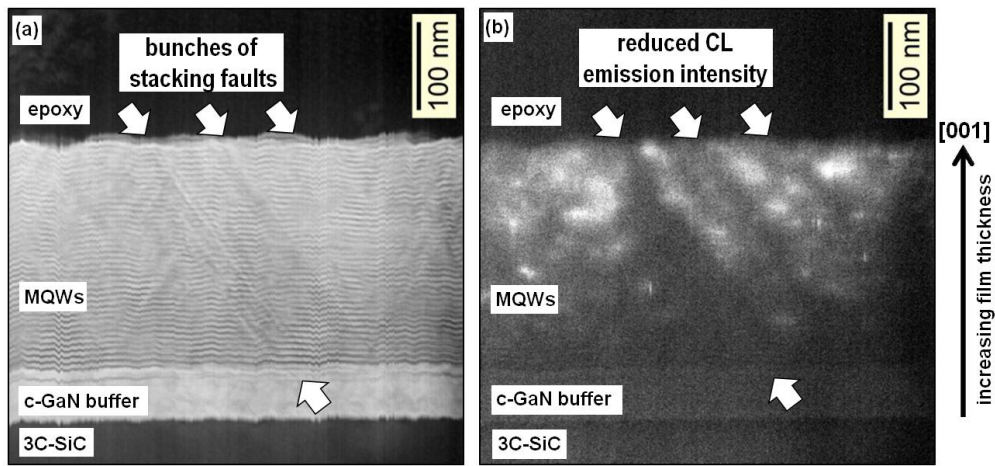


Figure 2 (a) Cross-sectional STEM image in HAADF contrast along the [110] zone axis of cubic GaN/AlN MQW sample. (b) Corresponding panchromatic image of the CL signal at room temperature.

The panchromatic (Fig. 2b) image reveals an inhomogeneous distribution of the CL emission intensity. The spatial correlation of Fig. 2a and b shows that the emission intensity increases with increasing MQW film thickness, i.e. towards the sample surface. High emission intensities (hot spots) appear in regions with a lower defect density, which are mostly located near the sample surface. In regions with bunches of SFs (marked with white arrows in Fig. 2a and b) the intensity of the CL signal is much lower and no hot spots can be detected here compared to areas with better crystal quality. In these regions, non-radiative recombination seems to be the predominant process. One reason for this could be non-radiative recombination centers induced by SFs. Another reason may be due to the wider band gap of the WZ GaN phase ($E_g=3.4$ eV) compared to the cubic phase ($E_g=3.2$ eV). Charge carriers induced in the WZ phase will diffuse into the surrounding cubic matrix with the smaller band gap. Near the interface to the

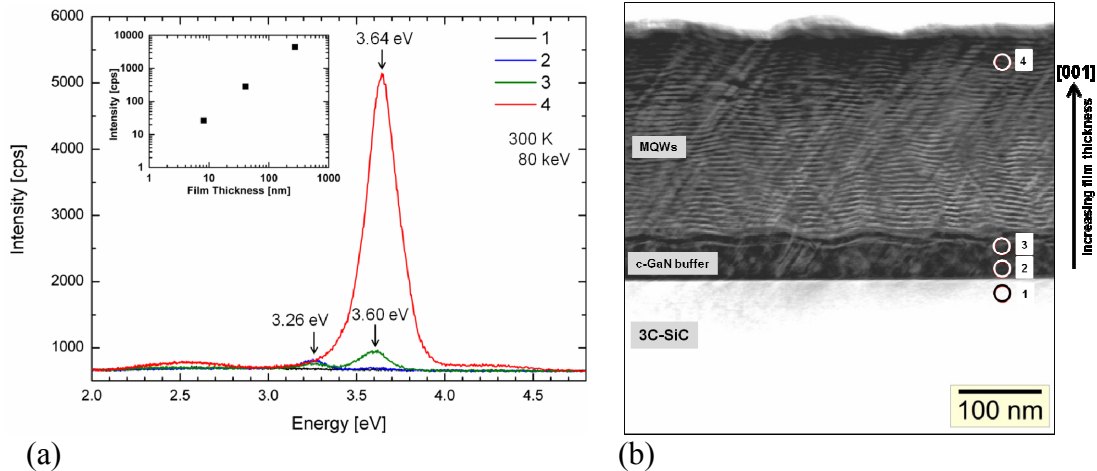


Figure 3 (a) Room temperature CL spectra 1-4 recorded at the marked regions 1-4 in the STEM image in (b). In the inset the maximum intensities of the MQW peak at 3.64 eV from spectra 2-4 are plotted *versus* the film thickness in a double logarithmic scale. **(b)** Cross-sectional ADF-STEM image taken along the [110] zone axis of the MQW sample.

3C-SiC substrate the CL emission intensity is obviously reduced. These measurements directly demonstrate a correlation between the CL emission intensity and the film thickness dependent crystal quality.

In Fig. 3a local room temperature CL spectra 1-4 taken from the MQW sample are displayed. The corresponding measurement spots 1-4 are marked in the STEM image in Fig. 3b and are ascending positioned with increasing film thickness. The CL emission spectrum 1 belongs to the 3C-SiC substrate, spectrum 2 to the c-GaN buffer layer, spectrum 3 to the area of the first c-AlN layer embedded in c-GaN and spectrum 4 was taken from the MQW layer near the surface of the sample, respectively. All emission spectra shown in Fig. 3a contain two dominant peaks at 3.26 eV and 3.64 eV plus the emission from the deep compensating complex in the range from 2.3-2.9 eV. The peak at 3.26 eV is due to the radiative recombination of the free exciton transition in c-GaN [15], and the emission peak at 3.64 eV can be related to the wider 2.1 nm QW of the asymmetric coupled c-MQWs [16].

In the inset of Fig. 3a the maximum intensities of the MQW peak at 3.64 eV from spectra 2-4 are plotted *versus* the film thickness in a double logarithmic scale. Here, the underground in Fig. 3a has been deducted from the maximum intensity values. A simple relationship between the film thickness and the MQW emission intensity is clearly observed pointing out that the emission intensity increases with decreasing defect density. These results are in good qualitative agreement with the observation that of the FWHM of the rocking curves also depends on the film thickness in c-GaN layers as observed in Ref. [17]. Therefore, we assume that the increasing CL emission intensity with increasing film thickness is correlated with a decreasing of the dislocation density N_{disl} . A systematic decrease of the SF density as a function of layer thickness has been also observed by the group of B. Daudin et al. [18].

The low temperature (16 K) CL measurements of the MQW structure are plotted in Fig 4. On the right side of Fig.4 a) a cross-sectional STEM image of the MQW sample is shown with a marked position of a line scan taken perpendicular from the sample surface towards the GaN/SiC interface. The line scan was taken over a range of 350 nm with a step size of 10 nm. On the left hand side of fig 4a a contour plot of normalized CL intensity over wavelength at each point of

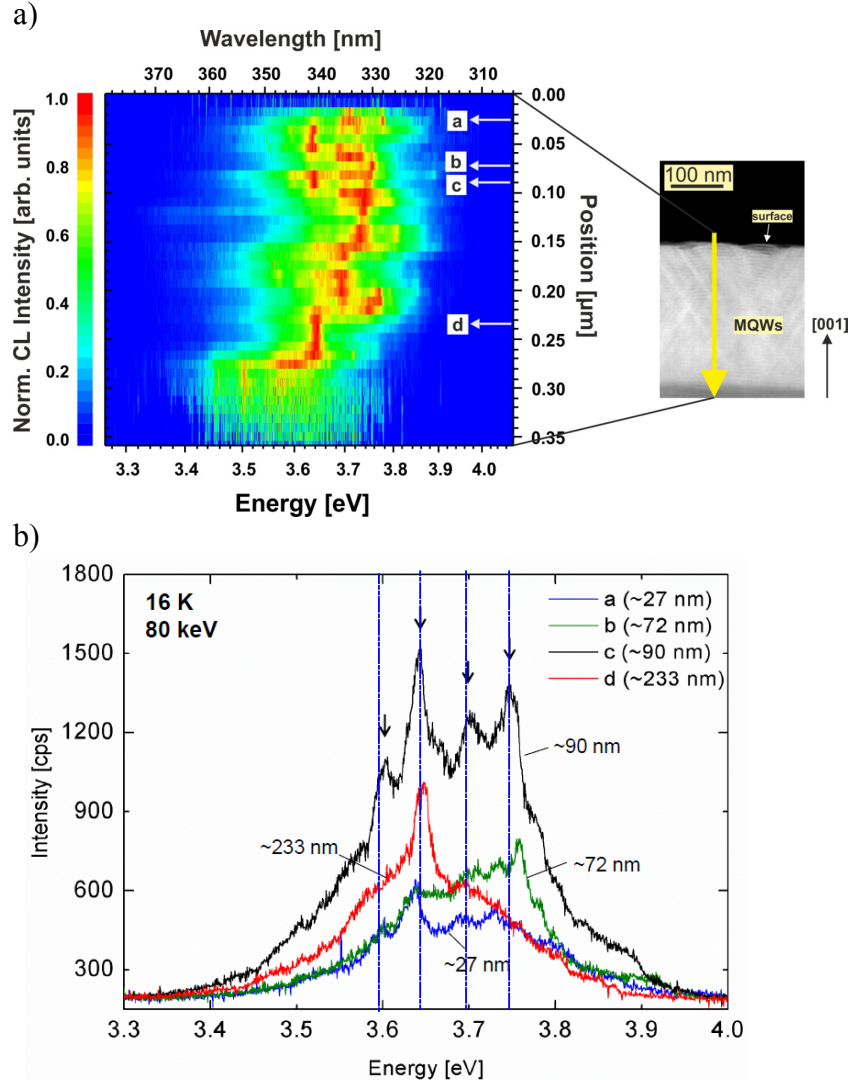


Figure 4 (a) Cross-sectional ADF-STEM image and line scan taken along the marked arrow. The line scan reveals the spectral evolution of the CL along the cross section at 16 K. (b) Extracted local CL emission spectra *a-d* from different positions (*a-d*) with associated measurement position in nm along the line scan marked in (a).

CONCLUSIONS

In summary, we have acquired and discussed correlated room temperature STEM/CL measurements from c-GaN/AlN MQWs films. An increasing CL emission intensity with increasing film thickness due to the improved crystal quality was observed. This correlation can be connected to the reduction of the FWHM of X-ray ω -rocking curves with increasing film thickness of c-GaN layers. Defects like SFs on the $\{111\}$ planes lead to a decrease of the CL emission intensity. With low temperature CL line scans also monolayer fluctuations of the QWs have been detected.

the line scan is shown. The color distribution of this line scan shows varying intensity maxima and a small red shift occurring from the sample surface towards the c-GaN buffer layer. In Fig. 4b local CL spectra *a-d* extracted from different positions (*a-d*) along the line scan in Fig. 4a are plotted. The local spectra contain several dominant emission maxima as indicated by arrows. These peaks are attributed to local thickness variation of the different thick QWs. The transition energies of the QWs have been simulated by the *nextnano3* software [19] and these calculations prove that the occurrence of these peaks is caused by monolayer fluctuations of the single MQW layers. The calculated transition energies for 7, 8, 9, and 10 ML thick GaN QWs are indicated in Fig. 4 b) by blue dashed lines, respectively.

ACKNOWLEDGMENTS

This work was supported by the DFG graduate program GRK 1464 “Micro- and Nanostructures in Optoelectronics and Photonics” and the TRR 142 “Tailored nonlinear photonics: From fundamental concepts to functional structures” as well as the Collaborative Research Center SFB 787 (project A8) and in the frame of the Research Instrumentation Program INST 272/148-1.

REFERENCES

1. P. Waltereit, O. Brandt, A. Trampert, H.T. Grahn, J. Menninger, M. Reiche, K.H. Ploog, *Nature* **406**, 865 (2000).
2. D.J. As, *Microelectronics Journal* **40**, 204 (2009).
3. S.V. Novikov, N.M. Stanton, R.P. Campion, C.T. Foxon, A.J. Kent, *J. Cryst. Growth* **310**, 3964 (2008).
4. G. Feuillet, F. Widmann, B. Daudin, J. Schuler, M. Arlery, J.L. Rouvière N. Pelekanos, O. Briot, *Materials Science and Engineering B* **50**, 233 (1997).
5. S. Sumnavadee, S. Sanorpim, B. Paosawat and K. Onabe, *J. of the Microscopy Society of Thailand* **24** (2), 136 (2010).
6. Th. D. Moustakas, *Phys. Status Solidi* (a) **210**, 169 (2013).
7. M. Albrecht, S. Christiansen, G. Salviati, C. Zanotti-Fregonara, Y. T. Rebane, Y. G. Shreter, M. Mayer, A. Pelzmann, M. Kamp, K. J. Ebeling, M. D. Bremser, R. F. Davis, and H. P. Strunk, *MRS Symp. Proc.* **468**, 293 (1997).
8. J. Lähnemann, O. Brandt, U. Jahn, C. Pfüller, C. Roder, P. Dogan, F. Grosse, A. Belabbes, F. Bechstedt, A. Trampert, and L. Geelhaar, *Phys. Rev. B* **86**, 081302(R) (2012).
9. R. Liu, A. Bell and F.A. Ponce, *Appl. Phys. Lett.* **86**, 021908 (2005).
10. F. Bertram, T. Riemann, J. Christen, A. Kaschner, A. Hoffmann, C. Thomsen, K. Hiramatsu, T. Shibata, and N. Sawaki, *Appl. Phys. Lett.* **74**, 359 (1999).
11. T. Chassagne, A. Leycuras, C. Balloud, P. Arcade, H. Peyre and S. Juillaguet, *Materials Science Forum Vols.* **457-460**, 273 (2004).
12. T. Schupp, K. Lischka and D.J. As, *J. of Cryst. Growth* **312**, 1500 (2010).
13. J. Schörmann, S. Potthast, D.J. As, K. Lischka, *Appl. Phys. Lett.* **90**, 041918 (2007).
14. R.M. Kemper, C. Mietze, L. Hiller, T. Stauden, J. Pezoldt, D. Meertens, M. Luysberg, D.J. As and J.K.N. Lindner, *Phys. Stat. Sol. (c)*, **11**, 265 (2014).
15. D.J. As, F. Schmilgus, C. Wang, B. Schöttker, D. Schikora, and K. Lischka, *Appl. Phys. Lett.* **70**, 1311 (1997).
16. T. Wecker, H. Hörich, M. Feneberg, R. Goldhahn, D. Reuter and D.J. As, *Phys. Stat. Sol. (b)*, (2014) (accepted).
17. R.M. Kemper, P. Veit, C. Mietze, A. Dempewolf, T. Wecker, J. Christen, J.K.N. Lindner and D.J. As: *Phys. Stat. Sol. (c)* (2014) (submitted)
18. E. Martinez-Guerrero, E. Bellet-Almalric, L. Martinet, G. Feuillet, H. Mariette, P. Holliger, C. Dubois, C. Bru-Chevallier, P. Aboughe Nze, T. Chassagne, G. Ferro, Y. Monteil and B. Daudin, *J. Appl. Phys.* **91**, 4983 (2002).
19. S. Birner, C. Schindler, P. Greck, M. Sabathil, and P. Vogl, *J. Comput. Electron.* **8**, 267 (2009).